INTERNATIONAL JOURNAL FOR NUMERICAL METHODS IN ENGINEERING, VOL. 25, 227–251 (1988)

PLASTIC AND VISCOPLASTIC FLOW OF VOID-CONTAINING METALS. APPLICATIONS TO AXISYMMETRIC SHEET FORMING PROBLEMS

E. OÑATE

Escuela Tecnica Superior de Ingenieros de Caminos, Canales y Puertos, Jorge Girona Salgado 31, 08034 Barcelona, Spain

M. KLEIBER

Institute Fundamental Technological Research, Warsaw, Poland

C. AGELET DE SARACIBAR

Escuela Tecnica Superior de Ingenieros de Caminos, Canales y Puertos, Jorge Girona Salgado 31, 08034 Barcelona, Spain

SUMMARY

A formal analogy between the equations of pure plastic and viscoplastic flow theory for void-containing metals and those of standard non-linear elasticity is presented. The formulation is particularized for the analysis of axisymmetric sheet metal forming problems using simple two node linear finite elements. Details of the treatment of friction and strain hardening phenomena, time increment computation and elastic effects are also given. Examples of the effect of void porosity on the hemispherical stretching of a circular sheet are presented.

INTRODUCTION

An effective way for developing computational models for problems of continuous deformation of metals is to treat the material as an incompressible viscous fluid of a non-Newtonian kind. This procedure, formally identical to that of pure viscoplasticity theory, is usually known as the 'flow approach' and it has been extensively used in recent years in conjunction with the finite element method for solving a variety of bulk and sheet metal forming problems.[1–7]

Much of the success of the finite element flow formulation is due to its simplicity. It is well known that, if inertia terms are neglected, the flow equations for a von Mises type of material are analogous to those of classical non-linear incompressible elasticity with velocities, strain rates and non-linear viscosity playing the role of displacements, strains and shear modulus of the equivalent elasticity model, respectively. This allows finite element computer programs for metal forming analysis to be directly obtained by a simple modification of standard finite element packages written for 2D and 3D elasticity.[1,3]

One of the weak points of the viscous flow approach is its inability to predict degradation and failure of the deforming material. Thus, important effects like metal fracture are, in principle, impossible to reproduce with the standard plastic or viscoplastic flow models.

In ductile metals softening and ultimate failure by nucleation, growth and coalescence of

0029–5981/88/010227–25$12.50

Received January 1987

microscopic voids are important fracture mechanisms. Voids nucleate mainly at second phase particles, by particle fracture or by interfacial decohesion, and subsequently the voids grow due to intensive plastic straining when the ligaments between neighbouring voids have thinned down sufficiently.

In this paper, the effect of nucleation, growth and coalescence of voids in the deformation of a plastic metal is studied. The layout of the paper is the following. In the next section it is shown how the equations of pure plastic flow of the voided metal are analogous to those of non-linear compressible elasticity. This allows finite element solutions to be obtained for such potentially difficult problems in a simple manner by directly using computer programs written for standard 2D and 3D elasticity. This formal analogy is shown to hold also for the case of viscous flow of a void-containing material.

In the sections which follow the flow formulation is particularized for the analysis of axisymmetric thin sheet metal forming problems and details of the corresponding shell and membrane formulations using simple two node axisymmetric elements are given.

Important aspects like the treatment of friction and strain hardening phenomena, time step computation and inclusion of elastic effects are also briefly discussed. Finally, examples of application to the hemispherical stretching of a circular sheet of metal, including the effect of voids, are presented.

PLASTICITY OF VOID-CONTAINING METALS

A rational model that describes the nucleation, growth and finally coalescence of voids in metals can be developed on the basis of the so-called Gurson model.[8] The model has the formal structure of non-associated plasticity equations with plastic dilatancy effects taken appropriately into account.[8–15] The ductile fracture process is described as an apparent loss of active material volume with a corresponding decay of the average macroscopic stress. Applications of this model for sheet metal forming problems using an elastoplastic formulation have been presented by Chu.[16] In the present study the effect of elasticity, of small importance in the presence of large plastic deformations, will be initially neglected. A procedure for dealing with elastic effects will be discussed in a later section.

The yield condition for a randomly voided material with spherical (for 3D problems) or circular cylindrical voids (for plane stress problems) may be assumed as[8]

$$\phi(\sigma_{ij}, \sigma_M, f) = \frac{3}{2}\frac{\sigma_{ij}^D \sigma_{ij}^D}{\sigma_M^2} + 2f\cosh\left(\frac{\sigma_{kk}}{2\sigma_M}\right) - (1+f^2) = 0 \tag{1}$$

where σ_{ij} is the microscopic Cauchy stress, σ_{ij}^D is the Cauchy stress deviator, σ_M is the tensile yield limit of the matrix material and f is the void volume fraction.

The summation convention is employed in (1). The matrix material is assumed incompressible. Note that for porosity parameter $f = 0$, equation (1) reduces to the classical von Mises yield condition of the form

$$\phi(\sigma_{ij}, \bar{\sigma}) = \frac{3}{2}\frac{\sigma_{ij}^D \sigma_{ij}^D}{\bar{\sigma}^2} - 1 = 0 \tag{2}$$

$\bar{\sigma} = \sigma_M$ being the current tensile yield limit. According to concepts discussed in References 8–15, the change of the void volume fraction during the increment of deformation is taken as

$$\dot{f} = \dot{f}_g + \dot{f}_n + \dot{f}_c \tag{3}$$

where subscripts g, n and c stand for growth, nucleation and coalescence of voids. Also, it can be

assumed that

$$\dot{f}_g = (1-f)\dot{\varepsilon}_{kk}^{(p)} \tag{4}$$

and the stress-controlled nucleation can be postulated in the form[9]

$$\dot{f}_n = \frac{k}{\sigma_M}\left(\dot{\sigma}_M + \frac{\dot{\sigma}_{kk}}{3}\right) \tag{5}$$

the material parameter k being the volume fraction of particles converted to voids per unit fractional increase in stress. Nucleation is assumed to occur only if the approximate value of the maximum normal stress $\sigma_M + \sigma_{kk}/3$ exceeds in the current time increment of its previous maximum. The term $\dot{f}_c$ in equation (3) will be discussed later.

After some routine calculations[8-14] it is possible to arrive at the typical non associated flow rule

$$\dot{\varepsilon}_{ij}^{(p)} = \frac{1}{\bar{\xi}}{}_1 s_{ij}({}_2 s_{kl}\dot{\sigma}_{kl}) \tag{6}$$

in which

$$\begin{aligned}
{}_1 s_{ij} &= \frac{3}{2}\frac{\sigma_{ij}^D}{\sigma_M} + \beta_1\delta_{ij} \\
{}_2 s_{ij} &= \frac{3}{2}\frac{\sigma_{ij}^D}{\sigma_M} + \beta_2\delta_{ij} \\
\beta_1 &= \frac{fS}{2} \\
\beta_2 &= \beta_1 + \frac{k}{6}\frac{\partial\phi}{\partial f} = \beta_1 + k\frac{C-f}{3} \\
\bar{\xi} &= \xi\frac{(w+fAS)^2}{1-f} - \frac{(C-f)\sigma_M}{2}\left[3f(1-f)S + 2\frac{k}{\sigma_M}\xi\frac{w+fAS}{1-f}\right]
\end{aligned} \tag{7}$$

where ξ is the classical isotropic hardening parameter for the matrix material

$$w = \frac{\bar{\sigma}^2}{\sigma_M^2} = \frac{\frac{3}{2}\sigma_{ij}^D\sigma_{ij}^D}{\sigma_M^2} = 1 - 2fC + f^2 \tag{8}$$

and

$$A = \frac{\sigma_{kk}}{2\sigma_M}, \quad S = \sinh A, \quad C = \cosh A \tag{9}$$

It can be easily seen that for standard plastic materials $f = 0$, $k = 0$ and $w = 1$, and then $\bar{\xi} = \xi$ and $\beta_1 = \beta_2 = 0$. Consequently, in this case the classical associated flow rule is obtained from equation (6) as

$$\dot{\varepsilon}_{ij}^{(p)} = \frac{1}{\xi}s_{ij}(s_{kl}\dot{\sigma}_{kl}) \tag{10}$$

with

$$s_{ij} = \frac{3}{2}\frac{\sigma_{ij}^D}{\bar{\sigma}} \tag{11}$$

Equation (10) can be rewritten in a more convenient form as

$$\dot{\varepsilon}_{ij}^{(p)} = \frac{1}{2\mu}\sigma_{ij}^{D} \tag{12}$$

where μ can be interpreted as the 'viscosity' of the equivalent viscous fluid, given by

$$\mu = \frac{\bar{\sigma}}{3\dot{\bar{\varepsilon}}^{(p)}} \tag{13}$$

with

$$\dot{\bar{\varepsilon}}^{(p)} = \sqrt{\tfrac{2}{3}\dot{\varepsilon}_{ij}^{(p)}\dot{\varepsilon}_{ij}^{(p)}} \tag{14}$$

Equations (12) and (13) are the basis of the standard 'plastic flow' approach which has been extensively used for the analysis of metal forming problems.[1-7] Note that in equation (13) the value of μ tends to infinity as $\dot{\bar{\varepsilon}}^{(p)}$ tends to zero, so in numerical computation a large but finite cut off value for μ must be assumed to allow for zones of rigid or nearly rigid behaviour.

ANALOGY OF THE PLASTIC VOIDED MATERIAL WITH STANDARD ELASTICITY

Using the expressions of ${}_1s_{ij}$ and ${}_2s_{ij}$ of equation (7), and after some algebra, equation (6) can be written as

$$\dot{\varepsilon}_{ij}^{(p)} = \frac{1}{\bar{\xi}}\bar{\alpha}\left[\frac{3}{2}\frac{\sigma_{ij}^{D}}{\sigma_M} + \beta_1\delta_{ij}\right] \tag{15}$$

with

$$\bar{\alpha} = \left(w\dot{\sigma}_M + \beta_2\dot{\sigma}_{kk} + \frac{\dot{w}\sigma_M}{2}\right) \tag{16}$$

The deviatoric stresses can be written as

$$\sigma_{ij}^{D} = \sigma_{ij} - p\delta_{ij} \tag{17}$$

where $p = \sigma_{kk}/3$ is the mean pressure.

Substituting equation (17) in (15), and using the value of β_1 of equation (7), it can finally be found that

$$\dot{\varepsilon}_{ij}^{(p)} = \frac{1}{2\bar{G}}[\sigma_{ij} - 2\bar{\nu}p\delta_{ij}] \tag{18}$$

with

$$\bar{G} = \frac{\sigma_M\bar{\xi}}{3\bar{\alpha}} \tag{19}$$

$$\bar{\nu} = \frac{1}{2}\left(1 - \frac{f}{2}\frac{\sinh A}{A}\right) \tag{20}$$

If we compare equation (18) with the constitutive equation for classical elasticity

$$\varepsilon_{ij} = \frac{1}{2G}\left[\sigma_{ij} - \frac{3\nu}{1+\nu}p\delta_{ij}\right] \tag{21}$$

where G and ν are the shear modulus and Poisson's ratio of the elastic material, respectively, we can

easily conclude that the equations for plastic flow of a voided metal are analogous to those of classical (compressible) elasticity. Therefore, standard finite element programs developed for 2D and 3D elasticity problems can be automatically used for the analysis of plastic deformation of voided metals by just replacing displacements and strains by velocities and strain rates, respectively, the shear modulus G by the parameter $\bar{G}$ of equation (19) and the Poisson's ratio ν by $2\bar{\nu}/(3-2\bar{\nu})$, with $\bar{\nu}$ given by equation (20). Note from equations (19) and (20) the stress and strain rate dependence of $\bar{G}$ and $\bar{\nu}$, which makes the analogous elastic problem non-linear. The numerical solution must therefore be found iteratively. However, in practice a simple direct iteration scheme is enough to reach convergence in a few iterations.

Equation (19) can be put in a much simpler form suitable for numerical computations. Thus, making use of equations (3)–(9), one can obtain

$$\bar{\alpha} = [w + fAS - k(C-f)]\bar{\xi}\dot{\bar{\varepsilon}}^{(p)} - (1-f)(C-f)\sigma_M \dot{\varepsilon}_{kk}^{(p)} - \dot{f}_c(C-f)\dot{\sigma}_M \tag{22}$$

Therefore, if the coalescence term is neglected, which is the case for values of $f < 0{\cdot}20$,[10] the expression for $\bar{\alpha}$ can be computed in terms of current values of strain rates, stresses, porosity and hardening modulus. Moreover, it can be found after some mathematics that the value of $\bar{G}$ for this case is given simply by

$$\bar{G} = \frac{\sigma_M}{3\dot{\bar{\varepsilon}}^{(p)}}\left(\frac{w + fAS}{1-f}\right) \tag{23}$$

which is a very convenient expression for use in the numerical process.

For classical plastic materials $w = 1, f = \beta_2 = \dot{w} = 0$ and $\sigma_M = \bar{\sigma}$, and therefore, from equations (23) (or (19)) and (20), we have

$$\bar{G} = \frac{\bar{\sigma}}{3\dot{\bar{\varepsilon}}^{(p)}} = \mu$$
$$\bar{\nu} = \nu = \tfrac{1}{2} \tag{24}$$

Thus, the incompressible form of the deformation is recovered, and the expression for $\bar{G}$ coincides with that of the viscosity of the standard plastic flow problem (see equation (13)).

Finally, the term $\dot{f}_c$ in equation (3) can be numerically accounted for in the following way. According to Reference 10 coalescence takes place at $f \simeq 0{\cdot}20$. Thus, an extremely simple yet effective numerical scheme can be used to reproduce this phenomenon if, at points for which $f = 0{\cdot}2$, a proportional increase in f is assumed for a number of fixed incremental steps ($\simeq 5$), up to $f = 1$, for which the material carrying capacity in that point is effectively zero.[11,13] Note that for this case the expressions of $\bar{G}$ and $\bar{\nu}$ given respectively by equations (19) and (20) must be used.

INCLUSION OF VISCOPLASTIC EFFECTS IN THE FLOW EQUATIONS OF VOID-CONTAINING METALS

In Reference 3 the analogy between equations of linear elasticity and those of rigid-plasticity has been shown to hold for non-voided materials also in the case of viscous properties of a plastic solid. For the lack of any meaningful theory describing the time-dependent behaviour within the framework of Gurson's model, a similar analogy can hardly be obtained for porous materials (an attempt presented in Reference 14 seems to be two complex algebraically to allow for such a derivation).

However, it seems that an approximate way of including viscous effects in a void-containing material could be accounted for by proceeding as follows.

Using the classical overstress concept of viscoplasticity[3] we can define

$$\kappa = \sqrt{\frac{3}{2}\frac{\sigma_{ij}^{\mathrm{D}}\sigma_{ij}^{\mathrm{D}}}{w}} - \sigma_{\mathrm{M}} \tag{25}$$

where $\sqrt{w}$ is introduced to make the overstress parameter zero in the non-viscous case (when $\sqrt{\frac{3}{2}\sigma_{ij}^{\mathrm{D}}\sigma_{ij}^{\mathrm{D}}} = \sqrt{w}\,\sigma_{\mathrm{M}}$; see equation (8)).

By postulating the expressions for the viscoplastic strain rate as

$$\begin{aligned} \dot{\varepsilon}_{ij}^{(\mathrm{vp})} &= \gamma \kappa^{n}{}_{1} s_{ij} \quad \text{for} \quad \kappa > 0 \\ \dot{\varepsilon}_{ij}^{(\mathrm{vp})} &= 0 \qquad\quad \text{for} \quad \kappa \leqslant 0 \end{aligned} \tag{26}$$

where γ is the material fluidity, we obtain

$$\dot{\bar{\varepsilon}}_{ij}^{(\mathrm{vp})} = \sqrt{\tfrac{2}{3}\dot{\varepsilon}_{ij}^{(\mathrm{vp})}\dot{\varepsilon}_{ij}^{(\mathrm{vp})}} = \gamma\kappa^{n}\sqrt{\tfrac{2}{31}s_{ij1}s_{ij}} = \gamma\kappa^{n}\sqrt{w + 2\beta_1^2} \tag{27}$$

Thus,

$$\left(\frac{\dot{\bar{\varepsilon}}_{ij}^{(\mathrm{vp})}}{\gamma\sqrt{w+2\beta_1^2}}\right)^{1/n} = \sqrt{\frac{3}{2}\frac{\sigma_{ij}^{\mathrm{D}}\sigma_{ij}^{\mathrm{D}}}{w}} - \sigma_{\mathrm{M}} \tag{28}$$

which can be considered as a viscous counterpart of the relation (equation (1))

$$\sqrt{\frac{3}{2}\frac{\sigma_{ij}^{\mathrm{D}}\sigma_{ij}^{\mathrm{D}}}{w}} - \sigma_{\mathrm{M}} = 0$$

It is seen that for finite values of the fluidity γ the current macro stresses σ_{ij} may now significantly exceed those allowed in Gurson's model—the excess stresses are bigger when strain rates are higher.

Let us rewrite the last equation as

$$\sigma_{\mathrm{M}}\left[1 + \left(\frac{\dot{\bar{\varepsilon}}^{(\mathrm{vp})}}{\gamma\sigma_{\mathrm{M}}^{n}\sqrt{w+2\beta_1^2}}\right)^{1/n}\right] = \sqrt{\frac{3}{2}\frac{\sigma_{ij}^{\mathrm{D}}\sigma_{ij}^{\mathrm{D}}}{w}} \tag{29}$$

Comparing it with the condition

$$\sigma_{\mathrm{M}} = \sqrt{\frac{3}{2}\frac{\sigma_{ij}^{\mathrm{D}}\sigma_{ij}^{\mathrm{D}}}{w}} \tag{30}$$

we see that accounting for viscous properties corresponds roughly speaking to replacing the matrix yield value σ_{M} by

$$\sigma_{\mathrm{M}}\left[1 + \left(\frac{\dot{\bar{\varepsilon}}^{(\mathrm{vp})}}{\gamma\sigma_{\mathrm{M}}^{n}\sqrt{w+2\beta_1^2}}\right)^{1/n}\right]$$

Using this observation we write equation (19) as

$$\bar{G} = \frac{\bar{\xi}\sigma_{\mathrm{M}}\left[1 + \left(\dfrac{\dot{\bar{\varepsilon}}^{(\mathrm{vp})}}{\gamma\sigma_{\mathrm{M}}^{n}\sqrt{w+2\beta_1^2}}\right)^{1/n}\right]}{3\bar{\alpha}} \tag{31}$$

An additional justification for the above *ad hoc* assumption stems from the fact that the last

equation for particular case of non-voided material ($w = 1, \beta_1 = 0, \beta_2 = 0$) leads to

$$\bar{G} = \frac{\bar{\sigma} + \left(\dfrac{\dot{\bar{\varepsilon}}^{(vp)}}{\gamma}\right)^{1/n}}{3\dot{\bar{\varepsilon}}^{(vp)}} \tag{32}$$

which exactly coincides with the relation derived in References 3 and 4. Thus, it seems that after appropiate calibration, the expression for $\bar{G}$ of equation (32) could be used in practical computations of void-containing viscoplastic materials since it accounts for all the basic ingredients required in such a case. Note that the simplified form of $\bar{G}$ given by equation (23) can again be effectively used with the new value of the matrix yield limit, σ_M, as explained above.

APPLICATION TO THIN SHEET METAL FORMING

The analogy presented in the previous section allows the immediate treatment of large plastic or viscoplastic deformations of voided thin sheets of metals making direct use of classical shell theory. The solution scheme is thus as follows.

(1) Identify an elastic shell formulation. If standard finite element techniques are used, a discrete system of equations is obtained, upon discretization, of the form[3,5,6]

$$\mathbf{K}\mathbf{a} = \mathbf{f} \tag{33}$$

where $\mathbf{K}$ is the shell stiffness matrix, and $\mathbf{a}$ and $\mathbf{f}$ are the displacement and nodal forces vectors, respectively. The equivalent 'viscous voided shell' is formulated by simply identifying displacements and strains with velocities and strain rates, respectively, and the shear modulus and Poisson's ratio with the parameters $\bar{G}$ and $2\bar{\nu}/(3-2\bar{\nu})$, respectively.

Equation (33) becomes a system of non-linear equations which must be solved iteratively. In the initial solution values of the velocities $\mathbf{a}^0$, void volume fraction f and parameters $\bar{G}$ and $\bar{\nu}$ are assumed.

(2) Solve for $\mathbf{a}^1$. If direct iteration is used, the first iteration becomes

$$\mathbf{a}^1 = [\mathbf{K}(\mathbf{a}^0)]^{-1}\mathbf{f} \tag{34}$$

(3) Check for convergence of velocities. If desired convergence is not achieved go back to (2).

(4) Once convergence has been achieved the geometry is updated by $\mathbf{a}\Delta t$, where Δt is an appropriate time step size. Also, the boundary conditions must be changed if new points of the sheet have come into contact with the tool surface. Finally, the sheet thickness and void volume fraction are also updated accordingly to the values of the thickness and volumetric strains, respectively.

(5) The process is restarted with the new values of the sheet geometry and void volume fraction.

The algorithm is thus very simple and it also allows other effects like strain hardening and friction conditions in the sheet/tool interface to be included in a straightforward manner as will be briefly explained later.

We have to note that direct iteration usually yields convergence of the velocity field after a small number of iterations. This is due to the well posed boundary value nature of the problem in which velocities are prescribed at the tool–blank contact nodes, and forces (reactions) are obtained '*a posteriori*' from the converged velocity field. Thus, for each solution the initial velocities can be guessed to be not too far from their correct values and convergence is rapidly achieved. Special care, however, must be taken to define a cut-off value of the equivalent shear modulus in zones of

the sheet with zero, or almost zero, porosity and where no rigid deformations are expected, to prevent ill conditioning of the stiffness matrix, as already mentioned (see equation (13)).

In the next sections we present details of the finite element viscous voided shell formulation for axisymmetric sheet metal forming problems.

FINITE ELEMENT AXISYMMETRIC VISCOUS VOIDED SHELL FORMULATION

In this section a finite element viscous shell formulation for the analysis of axisymmetric sheet forming processes including the effect of voids is presented. As previously explained, the basis of the success of such a formulation lies in the efficiency of the analogous elastic shell solution. We will use here the axisymmetric finite element shell formulation with simple two node linear elements developed by Zienkiewicz *et al.*[17] This formulation has been successfully used by Oñate and Zienkiewicz[5] for the analysis of thin sheet metal forming problems using the standard plastic flow approach.

The shell formulation is based on the following basic assumptions:

1) normals to the shell midsurface before deformation remain straight but not necessarily orthogonal to the midsurface after deformation;
2) the normal stress $\sigma_{z'}$ is negligible;
3) the term $(1 + t/R) \simeq 1$, where t and R are the shell thickness and radius of curvature, respectively;
4) the loading is also axisymmetric.

Velocity field

Assumption 1 allows the local velocities of a point to be expressed as (see Figure 1)

$$u' = u'_o - z'\theta$$
$$w' = w'_o \tag{35}$$

where z' is the co-ordinate in the thickness direction, index 'o' indicates midsurface velocities

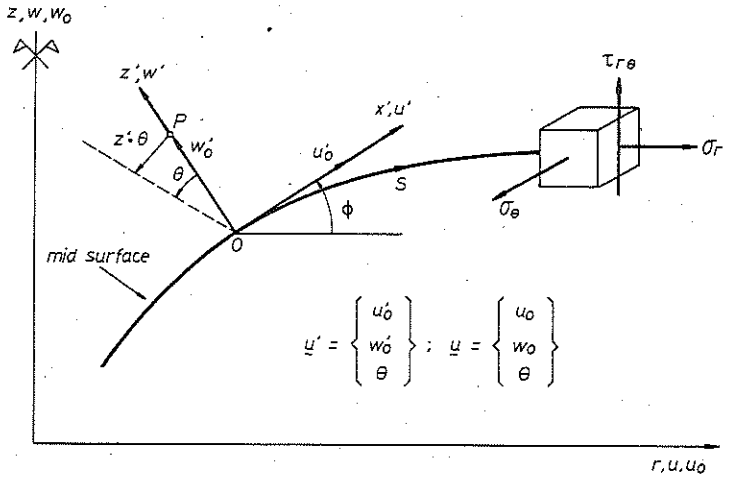

Figure 1. Axisymmetric shell. Geometry, velocity and stress field

and θ is the normal rotation velocity. Global and local velocities are related by

$$\mathbf{u} = \mathbf{T}\mathbf{u}' \quad \text{with} \quad \mathbf{T} = \begin{bmatrix} \cos\phi & -\sin\phi & 0 \\ \sin\phi & \cos\phi & 0 \\ 0 & 0 & 1 \end{bmatrix} \tag{36}$$

where vectors $\mathbf{u}$ and $\mathbf{u}'$ and angle ϕ are shown in Figure 1.

Strain rate field

The local strain rate vector is given by[17]

$$\dot{\boldsymbol{\varepsilon}} = \begin{Bmatrix} \dot{\varepsilon}_r \\ \dot{\varepsilon}_\theta \\ \dot{\gamma}_{r\theta} \end{Bmatrix} = \begin{Bmatrix} \dfrac{\partial u'}{\partial x'} \\ \dfrac{u}{r} \\ \dfrac{\partial w'}{\partial x'} + \dfrac{\partial u'}{\partial z'} \end{Bmatrix} \tag{37}$$

Using equations (35) and (36) and assumption 3, vector $\dot{\boldsymbol{\varepsilon}}$ can be written, after some transformations, as

$$\dot{\boldsymbol{\varepsilon}} = \begin{Bmatrix} \dot{\varepsilon}_r^0 + z'\dot{K}_r \\ \dot{\varepsilon}_\theta^0 + z'\dot{K}_\theta \\ \dot{\gamma}_{r\theta} \end{Bmatrix} = \mathbf{S}\hat{\dot{\boldsymbol{\varepsilon}}} \tag{38}$$

where

$$\hat{\dot{\boldsymbol{\varepsilon}}} = [\dot{\varepsilon}_r^0, \dot{\varepsilon}_\theta^0, \dot{K}_r, \dot{K}_\theta, \dot{\gamma}_{r\theta}]^{\mathrm{T}} \tag{39}$$

with

$$\begin{aligned} \dot{\varepsilon}_r^0 &= \cos\phi \frac{\partial u_0}{\partial s} + \sin\phi \frac{\partial w_0}{\partial s} \\ \dot{\varepsilon}_\theta^0 &= \frac{u_0}{r} \\ \dot{K}_r &= -\frac{\partial \theta}{\partial s} \\ \dot{K}_\theta &= -\frac{\theta \cos\phi}{r} \\ \dot{\gamma}_{r\theta} &= -\sin\phi \frac{\partial u_0}{\partial s} + \cos\phi \frac{\partial w_0}{\partial s} - \theta \end{aligned} \tag{40}$$

and

$$\mathbf{S} = \begin{bmatrix} 1 & 0 & z' & 0 & 0 \\ 0 & 1 & 0 & z' & 0 \\ 0 & 0 & 0 & 0 & 1 \end{bmatrix} \tag{41}$$

In (39) $\hat{\dot{\boldsymbol{\varepsilon}}}$ is the generalized strain rate vector and $(\dot{\varepsilon}_r^0, \dot{\varepsilon}_\theta^0), (\dot{K}_r, \dot{K}_\theta)$ and $\dot{\gamma}_{r\theta}$ correspond to membrane, flexural and shear generalized strain rates, respectively.

Stress field. Constitutive equation

The constitutive equation relating stresses and strain rates is directly obtained from standard plane stress elasticity[17] and the relationships between G and ν with $\bar{G}$ and $\bar{\nu}$ explained previously, as

$$\boldsymbol{\sigma} = [\sigma_r, \sigma_\theta, \tau_{r\theta}]^{\mathrm{T}} = \mathbf{D}\dot{\boldsymbol{\varepsilon}} \tag{42}$$

For an isotropic material

$$\mathbf{D} = \begin{bmatrix} d_{11} & d_{12} & 0 \\ d_{21} & d_{22} & 0 \\ 0 & 0 & d_{33} \end{bmatrix}$$

with

$$d_{11} = d_{22} = \frac{2\bar{G}(3-2\bar{\nu})}{(3-4\bar{\nu})}$$

$$d_{12} = d_{21} = \frac{4\bar{G}\bar{\nu}}{3-4\bar{\nu}} \tag{43}$$

$$d_{33} = \bar{G}$$

where $\bar{G}$ and $\bar{\nu}$ are given by equations (19) and (20), respectively. For the sign criterion of the stresses, see Figure 1.

Virtual work equation

The equation of virtual velocities is written as

$$2\pi \int_0^s \int_{-t/2}^{+t/2} \delta\dot{\boldsymbol{\varepsilon}}^{\mathrm{T}} \boldsymbol{\sigma} r \, \mathrm{d}s \, \mathrm{d}z' = 2\pi \int_0^s \delta\mathbf{u}^{\mathrm{T}} \bar{\mathbf{t}} r \, \mathrm{d}s + 2\pi \sum_j \delta\mathbf{u}_j^{\mathrm{T}} \mathbf{p}_j r_j \tag{44}$$

where $\bar{\mathbf{t}}$ and $\mathbf{p}_j$ correspond to surface and point load vectors, respectively. The left hand side of (44) can be rewritten using equations (38) and (42) as

$$2\pi \int_0^s \int_{-t/2}^{+t/2} \delta\dot{\boldsymbol{\varepsilon}}^{\mathrm{T}} \boldsymbol{\sigma} r \, \mathrm{d}s \, \mathrm{d}z' = 2\pi \int_0^s \delta\hat{\boldsymbol{\varepsilon}}^{\mathrm{T}} \hat{\mathbf{D}} \hat{\boldsymbol{\varepsilon}} r \, \mathrm{d}s \tag{45}$$

where

$$\hat{\mathbf{D}} = \int_{-t/2}^{+t/2} \mathbf{S}^{\mathrm{T}} \mathbf{D} \mathbf{S} \, \mathrm{d}z' = \int_{-t/2}^{+t/2} \begin{bmatrix} \mathbf{D}_{\mathrm{m}} & z'\mathbf{D}_{\mathrm{m}} & 0 \\ z'\mathbf{D}_{\mathrm{m}} & (z')^2\mathbf{D}_{\mathrm{m}} & 0 \\ 0 & 0 & d_{33} \end{bmatrix} \mathrm{d}z' \tag{46}$$

and

$$\mathbf{D}_{\mathrm{m}} = \begin{bmatrix} d_{11} & d_{12} \\ d_{12} & d_{22} \end{bmatrix} \tag{47}$$

with d_{11}, d_{12} and d_{22} having been defined in equation (43). For further use we also define

$$\hat{\mathbf{D}}_{\mathrm{m}} = \int_{-t/2}^{+t/2} \mathbf{D}_{\mathrm{m}} \, \mathrm{d}z'; \qquad \hat{\mathbf{D}}_{\mathrm{mb}} = \int_{-t/2}^{+t/2} z'\mathbf{D}_{\mathrm{m}} \, \mathrm{d}z'$$

$$\hat{\mathbf{D}}_{\mathrm{b}} = \int_{-t/2}^{+t/2} (z')^2 \mathbf{D}_{\mathrm{m}} \, \mathrm{d}z' \quad \text{and} \quad \hat{\mathbf{D}}_{\mathrm{s}} = \int_{-t/2}^{+t/2} d_{33} \, \mathrm{d}z' \tag{48}$$

where $\hat{\mathbf{D}}_{\mathrm{m}}$, $\hat{\mathbf{D}}_{\mathrm{mb}}$, $\hat{\mathbf{D}}_{\mathrm{b}}$ and $\hat{\mathbf{D}}_{\mathrm{s}}$ are the resultant constitutive matrices for membrane, bending–membrane coupling, bending and shear effects, respectively.

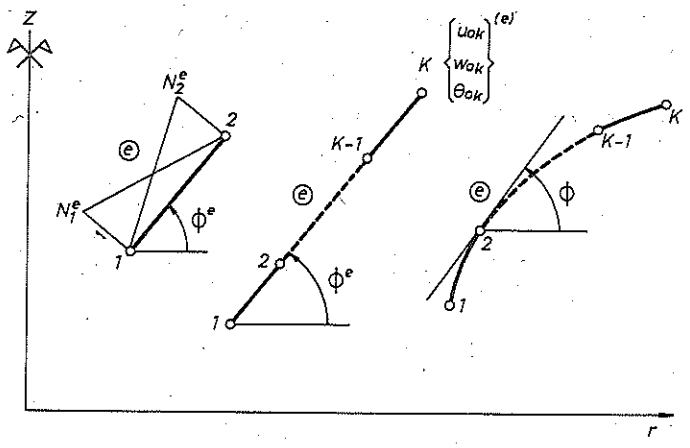

Figure 2. Straight and curved one dimensional elements for axisymmetric shell analysis

Finite element discretization. Linear element

With the above shell formulation we note that a finite element interpolation involving only continuity of the velocity field is required. Thus, any of the C_0 isoparametric one dimensional finite element interpolations are possible. Based on previous experiences,[5,17] we have chosen here the simple two node linear element of Figure 2. Therefore, the velocity field is expressed as

$$\mathbf{u} = \sum_{i=1}^{2} \mathbf{N}_i \mathbf{a}_i \tag{49}$$

where

$$\mathbf{N}_i = N_i \mathbf{I}_3 \quad \text{and} \quad \mathbf{a}_i = [u_{oi}, w_{oi}, \theta_i]^{\mathrm{T}} \tag{50}$$

In (50) N_i and $\mathbf{a}_i$ are the linear shape function (see Figure 2) and the vector of global velocities of node i, and $\mathbf{I}_3$ is the 3×3 unit matrix.

The generalized strain rate vector of equation (39) can be expressed in terms of the element nodal velocities as

$$\hat{\boldsymbol{\varepsilon}} = \sum_{i=1}^{2} \mathbf{B}_i \mathbf{a}_i \tag{51}$$

where

$$\mathbf{B}_i = \begin{Bmatrix} \mathbf{B}_{mi} \\ \hline \mathbf{B}_{bi} \\ \hline \mathbf{B}_{si} \end{Bmatrix} = \left[\begin{array}{ccc} \cos\phi \dfrac{\partial N_i}{\partial s} & \sin\phi \dfrac{\partial N_i}{\partial s} & 0 \\ \dfrac{N_i}{r} & 0 & 0 \\ \hline 0 & 0 & -\dfrac{\partial N_i}{\partial s} \\ 0 & 0 & -N_i \dfrac{\cos\phi}{r} \\ \hline -\sin\phi \dfrac{\partial N_i}{\partial s} & \cos\phi \dfrac{\partial N_i}{\partial s} & -N_i \end{array}\right] \tag{52}$$

In (52) $\mathbf{B}_{mi}$, $\mathbf{B}_{bi}$ and $\mathbf{B}_{si}$ are the membrane, bending and shear contributions to the nodal strain rate matrix $\mathbf{B}_i$.

Equations (49) and (51) can be used to obtain the standard discretized system of equilibrium equations upon substitution in the virtual work expression as

$$\mathbf{K}\mathbf{a} = \mathbf{f} \tag{53}$$

where the element contribution to the stiffness matrix $\mathbf{K}$ and the nodal force vector $\mathbf{f}$ are

$$\begin{aligned} \mathbf{K}_{ij}^{(e)} &= 2\pi \int_{l^{(e)}} \mathbf{B}_i^{\mathrm{T}} \hat{\mathbf{D}} \mathbf{B}_j r \, ds \\ \mathbf{f}_i^{(e)} &= 2\pi \int_{l^{(e)}} \mathbf{N}_i \mathbf{t} r \, ds + 2\pi r_i \mathbf{p}_i \end{aligned} \tag{54}$$

where $l^{(e)}$ is the element length.

Note that owing to the strain dependence of $\bar{G}$ and $\bar{\nu}$ parameters, the computation of the stiffness matrix implies a double integral (see equations (54) and (46)). This is in practice performed using numerical integration.

It has been shown[17] that for a successful use of the linear axisymmetric shell element for thin situations, one point Gaussian quadrature must be used for the integration of $\mathbf{K}_{ij}^{(e)}$ along the element length.[17] This allows one to obtain an explicit form of $\mathbf{K}_{ij}^{(e)}$ as

$$\mathbf{K}_{ij}^{(e)} = 2\pi \bar{\mathbf{B}}_i^{\mathrm{T}} \hat{\bar{\mathbf{D}}} \bar{\mathbf{B}}_j \bar{r} l^{(e)} \tag{55}$$

where the bar denotes values at the element mid point.

Matrix $\bar{\mathbf{B}}_i$ is readily obtained by substituting the terms N_i and $\partial N_i/\partial s$ in equation (52) by $1/2$ and $(-1)^i/l^{(e)}$, respectively.

It is worth pointing out that computation of $\hat{\mathbf{D}}$ still involves a numerical integration across the thickness for evaluating the integral of equation (46) at the element mid point. However, for well developed forming stages in which membrane effects dominate the solution,[6] a single Gaussian point across the thickness suffices for a precise evaluation of equation (46).

The membrane, membrane–bending coupling, bending and shear contributions to the stiffness matrix $\mathbf{K}_{ij}^{(e)}$ can be deduced from equations (46), (52) and (54) as

$$\begin{aligned} \mathbf{K}_{ij}^{(e)} = & \int_{-t/2}^{+t/2} \mathbf{B}_{mi}^{\mathrm{T}} \hat{\mathbf{D}}_{\mathrm{m}} \mathbf{B}_{mj} r \, ds + \int_{-t/2}^{+t/2} (\mathbf{B}_{mi}^{\mathrm{T}} \hat{\mathbf{D}}_{\mathrm{mb}} \mathbf{B}_{bj} + \mathbf{B}_{bi}^{\mathrm{T}} \hat{\mathbf{D}}_{\mathrm{mb}} \mathbf{B}_{mj}) r \, ds \\ & + \int_{-t/2}^{+t/2} \mathbf{B}_{bi}^{\mathrm{T}} \hat{\mathbf{D}}_{\mathrm{b}} \mathbf{B}_{bj} r \, ds + \int_{-t/2}^{+t/2} \mathbf{B}_{si}^{\mathrm{T}} \hat{\mathbf{D}}_{\mathrm{s}} \mathbf{B}_{sj} r \, ds \\ & = \mathbf{K}_{mij}^{(e)} + \mathbf{K}_{mbij}^{(e)} + \mathbf{K}_{bij}^{(e)} + \mathbf{K}_{sij}^{(e)} \end{aligned} \tag{56}$$

AXISYMMETRIC VISCOUS VOIDED MEMBRANE FORMULATION

The viscous membrane formulation can be easily derived from the general case presented in the previous sections by simply neglecting in all expressions the bending and shear terms. Therefore, the relevant matrices and vectors are now defined as

velocity vector: $\mathbf{u} = [u_o, w_o]^{\mathrm{T}}$ (57a)

generalized strain rate vector: $\hat{\boldsymbol{\varepsilon}} = [\hat{\varepsilon}_r, \hat{\varepsilon}_\theta]^{\mathrm{T}}$ (57b)

stress vector: $\boldsymbol{\sigma} = [\sigma_r, \sigma_\theta]^{\mathrm{T}}$ (57c)

constitutive matrices: $$\mathbf{D} = \mathbf{D}_m;\ \hat{\mathbf{D}} = t\mathbf{D}_m \tag{57d}$$

where $\mathbf{D}_m$ was given in equation (47). Note that equation (57d) is a direct consequence of the independence of material properties from the thickness co-ordinate, as it is in classical membrane theory. Finally, the explicit expression of the stiffness matrix for the linear element is given simply by

$$\mathbf{K}_{ij}^{(e)} = 2\pi \bar{\mathbf{B}}_{mi}^{T} \bar{\mathbf{D}} \bar{\mathbf{B}}_{mj}\, \bar{t}\bar{r}l^{(e)} \tag{58}$$

where the bar again denotes values at the element mid point.

TIME INCREMENT COMPUTATION AND GEOMETRY UPDATING

As already mentioned, in sheet forming problems a continuous updating of co-ordinates is obviously necessary to follow the sheet geometry changes. This implies that the sheet geometry has to be updated every time convergence of the velocity field is achieved and the limit of the blank/tool contact surface subsequently adjusted.

We will be concerned here with the calculation of the time increment for which the first node of the non-contacting region comes into contact with an indenting hemispherical punch; however, the same procedure could be applied to study the contact with the fixed tooling region.

The equation of the punch in the co-ordinate axes of Figure 3 is

$$r^2 + z^2 = R_p^2 \tag{59}$$

where R_p is the punch radius. If (r_4, z_4) and $(u_4, \bar{w}_4)$ are respectively the co-ordinates and velocities of the next node to come into contact (see Figure 3) at time t, the new co-ordinates (r'_4, z'_4) at time $t + \Delta t$ will be

$$\begin{aligned} r'_4 &= r_4 + u_4 \Delta t \\ z'_4 &= z_4 + (\bar{w}_4 - \bar{w}_p)\Delta t \end{aligned} \tag{60}$$

where $\bar{w}_p$ is the punch velocity. From Figure 3 we see that node 4 will come into contact when

$$z'_4 = z_1 \tag{61}$$

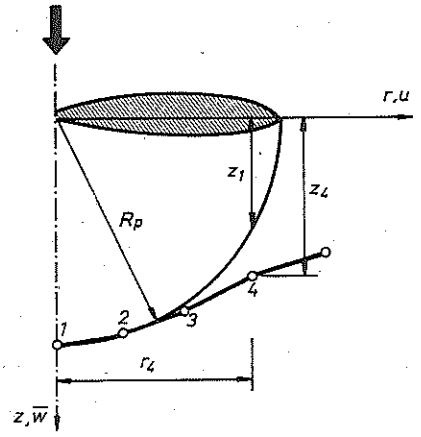

Figure 3. Co-ordinate axes for time step computation

The value of z_1 at time $t + \Delta t$ is obtained from equation (59). Therefore node 4 will come into contact if

$$z_4 + (\bar{w}_4 - \bar{w}_p)\Delta t = \sqrt{R_p^2 - (r_4 + u_4 \Delta t)^2} \tag{62}$$

which is a non-linear equation in Δt. If direct iteration is used, we have

$$\Delta t^{n+1} = \frac{\sqrt{R_p^2 - (r_4 + u_4 \Delta t)^2} - z_4}{\bar{w}_4 - \bar{w}_p} \tag{63}$$

The process stops when

$$\frac{\Delta t^n - \Delta t^{n-1}}{\Delta t^n} \leqslant 0{\cdot}01 \tag{64}$$

Convergence of the above computations has proved to be very fast and inexpensive.

The simplest updating procedure is to use the time step calculated in equation (63) to increment the blank co-ordinates by $\mathbf{a}\Delta t$ to their new deformed position so that we can be sure that the deformed blank does not cross the punch surface. However, the use of large time steps leads to instability and usually a small fraction of the time step calculated in equation (63) must be used.

An alternative procedure which has proved to be very efficient is to use a fixed time step Δt throughout the analysis and calculate the position of the next contact point, which, obviously, in general it will not coincide with the next free node. Once the position of the contact point has been obtained the finite element mesh is slightly modified so that the closest node is displaced to coincide with the contact point.

This method has the advantage that for each time step the contact region is modified in a simple manner, thus avoiding the numerical oscillations which occur when the contact points are limited to the nodes and the distance between them is not sufficiently small. Obviously, the time step chosen should not be so large that the next contact point lies outside the next free element of the non-contacting region.

USE OF CONSTANT SPATIAL VELOCITY FIELD

It can be easily checked that in most sheet forming problems the 'spatial' velocity field does not change much between two consecutive solutions once the forming process reaches a well developed stage. Consider, for example, the case shown by Baynham and Zienkiewicz[18] of the deep drawing of a circular sheet with a flat bottom punch. Figure 4 shows the shape of the blank at two positions of the punch (δ apart) for a well developed process (that is one where punch displacement is greater than the sum of the punch and die profile radii). If the radial and axial components of instantaneous velocity for the two blank geometries are plotted against the radial co-ordinate (see Figure 4) it is found that the shape of the curve is very similar for the two punch positions.

If, however, the velocity of a particular point of the blank is compared at two punch travel positions (for example, by plotting the velocity against the radius of the blank in the first position) it is found that some parts of the blank undergo a severe change of velocity. Such a comparison is made in Figure 4 and, clearly, the points which undergo the greatest change of velocity are those near the die profile radius.

Thus, if a Lagrangian approach is employed in which the velocity of the material points is used to update the blank geometry, the time steps Δt must be small. On the other hand, if a Eulerian approach is used in which the constant spatial velocity field is used to update the geometry, then the same velocity field can be used for a greater length of time and so the number of resolutions is reduced significantly.

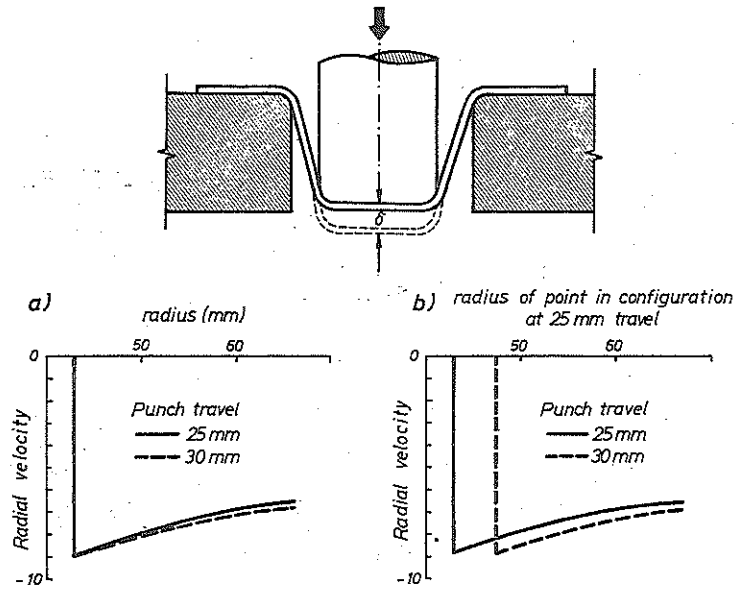

Figure 4. Radial velocity of material of blank: (a) spatial velocity field; (b) material velocity field for punch positions δ apart[18]

In this paper this latter method is used in combination with the constant time step algorithm, shown in the last section, as follows.

(a) Once the velocity field has been obtained for a blank position, a record is kept of the spatial velocity field in that particular position, which is taken as 'initial' in the following updatings of the blank.
(b) The blank geometry is updated using the spatial velocity field with a constant time step. After each updating the geometry of the blank is checked and modified so that it follows the tooling and punch profiles.
(c) Step (b) is repeated a few times using the same spatial velocity field. However, after a number of time steps the new converged velocity field must be computed for a more precise evaluation of punch force and blank strains.

TREATMENT OF FRICTION

The algorithm used to simulate friction effects between the contact interfaces is more complex than for continuum problems where non-directional friction laws can be introduced.[3] Here we have used a treatment of friction based on the iterative adjustment of nodal reactions corresponding to contact blank punch/tool nodes until they satisfy a Coulomb type of friction law. Thus, at the end of each iteration the reactions at each contact node in a 'friction co-ordinate system' are checked. If the value of the force along the slippage direction (the $\bar{u}_i$ direction in Figure 5) exceeds the value of the normal force times a friction coefficient, the node is allowed to slip in the appropriate direction and a prescribed friction force is applied at the node. The normal velocity of the node is then constrained to the value of the normal velocity of the punch, or to zero if the node is in contact with a fixed point of the tool/punch. Friction boundary conditions require that a transformation of the equilibrium equations at the friction co-ordinate system, defined in the direction of velocities $\bar{u}_i$ and $\bar{w}_i$ in Figure 5 (where direction $\bar{u}_i$ is the average of the directions of two elements meeting at the

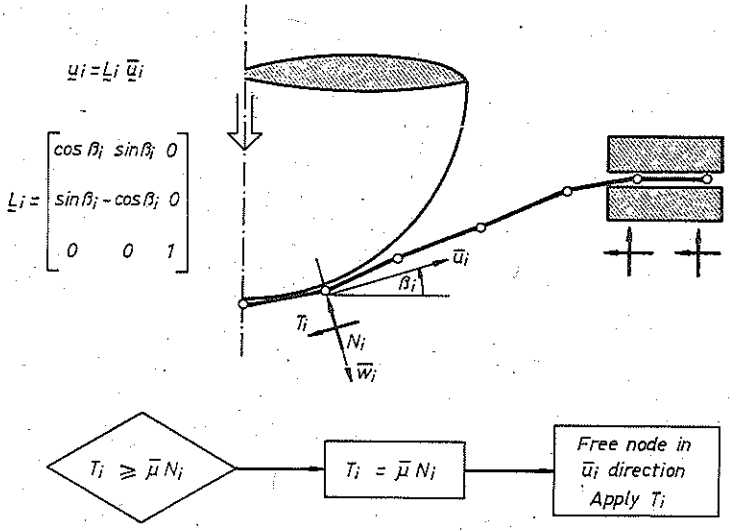

Figure 5. Treatment of friction

contact node i), must be performed, so that the friction boundary conditions in velocities and forces can be appropriately imposed or checked. The new stiffness matrix of the element in the friction co-ordinate system $\bar{\mathbf{K}}_{ij}$ is obtained by the standard transformation

$$\bar{\mathbf{K}}_{ij}^{(e)} = \mathbf{L}_i^{\mathrm{T}} \mathbf{K}_{ij}^{(e)} \mathbf{L}_j \tag{65}$$

where $\mathbf{K}_{ij}^{(e)}$ is given by equation (54) and matrix $\mathbf{L}_i$ is shown in Figure 5.

Equation (65) allows velocities and forces at the contact node in the friction co-ordinate system to be obtained, thus allowing for an easy checking of the friction forces and a direct prescription of the adequate boundary conditions. On the other hand, once the convergence of the solution has been achieved, velocities and forces are transformed into their Cartesian nodal components using matrix $\mathbf{L}_i$.

STRAIN HARDENING EFFECTS

The change of yield strength with the deformation process is easily included in the calculation. In most cases the yield stress is a function of the total effective strain invariant. For Lagrangian (material) co-ordinates computation of $\bar{\varepsilon}$ can be found by direct integration of the corresponding rate $\dot{\bar{\varepsilon}}$ defined by

$$\frac{\partial \bar{\varepsilon}}{\partial t} = \dot{\bar{\varepsilon}} \tag{66}$$

Thus, at each stage of the deformation the value of $\bar{\varepsilon}$ can be simply evaluated as

$$\bar{\varepsilon}^{t+\Delta t} = \bar{\varepsilon}^{t} + \int_{t}^{t+\Delta t} \dot{\bar{\varepsilon}}\, \mathrm{d}t \simeq \bar{\varepsilon}^{t} + \dot{\bar{\varepsilon}}\, \Delta t \tag{67}$$

and the yield stress appropriately updated.

INCLUSION OF ELASTIC EFFECTS IN THE VISCOUS VOIDED SHELL FORMULATION

The viscous shell formulations presented in previous sections exclude elastic effects by the nature of the constitutive relations assumed in the viscous flow approach. This implies that the removal of loads is not accompanied by an elastic springback, and therefore, the resulting residual stresses can not be calculated.

One simple procedure for recovery of residual stresses is to assume that the removal of the forces from the final viscous configuration is purely elastic and is resolved by a small deformation elastic (or elastoplastic) program. This procedure, originally presented by Zienkiewicz *et al.*,[3] introduces some approximations since the influence of the elastic deformation in the final sheet shape is ignored. This, however, is of little significance in most sheet metal deformation problems.

Nevertheless, inclusion of elastic effects may be of interest in some situations and below we generalize a procedure suggested by Zienkiewicz[7] and Thompson and Berman[7] for dealing with elastic effects in the viscous voided shell formulation.

If elastic effects are included the total strain rate is given by

$$\dot{\varepsilon}_{ij} = \dot{\varepsilon}_{ij}^{(e)} + \dot{\varepsilon}_{ij}^{(p)} \tag{68}$$

On the other hand, if we assume that the elastic deformations are incompressible we can write

$$\dot{\varepsilon}_{ij}^{(e)} = \frac{1}{2G} \overset{\nabla}{\sigma}{}_{ij}^{D} \tag{69}$$

where G is the elastic shear modulus and $\overset{\nabla}{\sigma}{}_{ij}^{D}$ is the co-rotational (or Jaumann) derivative of the deviatoric Cauchy stress. For updated Lagrangian problems such derivatives are given by

$$\overset{\Delta}{\sigma}{}_{ij}^{D} = \omega_{ij}\sigma_{kj}^{D} + \omega_{jk}\sigma_{ki}^{D} + \frac{\partial \sigma_{ij}^{D}}{\partial t} \tag{70}$$

where

$$\omega_{ij} = \tfrac{1}{2}(u_{j,i} - u_{i,j}) \tag{71}$$

is the rigid body rotation rate caused by the motion. Equation (70) simply takes into account stress changes associated with rotation of the axes of the material. The assumption of compressible elastic effects is also possible and this simply implies a modification of equation (69) to account for the effect of Poisson's ratio.

From equations (68) and (18) we obtain

$$\boldsymbol{\sigma} = \mathbf{D}(\hat{\boldsymbol{\varepsilon}} - \hat{\boldsymbol{\varepsilon}}^{(e)}) \tag{72}$$

where $\mathbf{D}$ is the equivalent elasticity matrix of the viscous voided material obtained in terms of $\bar{G}$ and $\bar{\nu}$ parameters, as explained in previous sections.

Equation (72) shows that if the elastic strain rate is assumed to be known from the previous iteration the problem is similar to the classical initial stress method in which the additional stress terms $-\mathbf{D}\dot{\boldsymbol{\varepsilon}}^{(e)}$ are added to the equilibrium flow equations as an 'unbalanced force' and connected. Thus, the discretized equilibrium equations have the form

$$\mathbf{K}\mathbf{a} = \mathbf{f} + \mathbf{f}_o \tag{73}$$

where $\mathbf{K}$ and $\mathbf{f}$ are the stiffness matrix and force vector for the flow approach and the extra force vector $\mathbf{f}_o$ is given for the axisymmetric viscous shall case as

$$\mathbf{f}_o = 2\pi \int_{l^{(e)}} \mathbf{B}^T \mathbf{D} \hat{\boldsymbol{\varepsilon}}^{(e)} r \, ds \tag{74}$$

where $\hat{\boldsymbol{\varepsilon}}^{(e)}$ is obtained from equations (39) and (69).

The iterative solution of equation (73) may prove to be not convergent if the effects of elasticity are large, but the exact limits have yet to be determined. Research in this area is currently being developed by the authors.

EXAMPLES

The efficiency of the formulation presented in previous sections is checked with a well known example of hemispherical stretching of a circular isotropic sheet for which experimental results are available.[19]

The geometrical configuration of the problem is shown in Figure 6. Fifty linear elements have been used for the analysis. The uniaxial stress-effective strain curve of the matrix material is given by

$$\bar{\sigma} = 5{\cdot}4 + 27{\cdot}8\,\bar{\varepsilon}^{0{\cdot}504}\ \text{tons/in}^2, \quad \bar{\varepsilon} < 0{\cdot}36$$

$$\bar{\sigma} = 5{\cdot}4 + 24{\cdot}4\,\bar{\varepsilon}^{0{\cdot}375}\ \text{tons/in}^2, \quad 0{\cdot}36 < \bar{\varepsilon}$$

$$\bar{\sigma} = 22{\cdot}0\ \text{tons/in}^2; \qquad \bar{\sigma} > 22{\cdot}0$$

In the first case studied a friction coefficient of 0·04 has been used, as suggested in Reference 19. The problem has been analysed for different initial void volume fractions of $f_0 = 0{\cdot}00, 0{\cdot}01$ and 0·05, and nucleation parameters $k = 0{\cdot}00$ and 0·02 in all elements. Numerical results for the punch load–displacement curves for various values of f_0 and k are shown in Figure 7(a). From these results it can be deduced that:

(a) An increase of the initial void porosity and nucleation parameters causes a progressive reduction of the load carrying capacity of the sheet. Values of the maximum punch load obtained for $f_0 = 0{\cdot}00$ and 0·01 with $k = 0{\cdot}0$ and 0·02, and $f_0 = 0{\cdot}05$ with $k = 0{\cdot}00$, are in agreement with the experimental results reported in Reference 19. However, for $f_0 = 0{\cdot}05$ and $k = 0{\cdot}02$ a reduction of the maximum punch load of 35 per cent is obtained.

(b) Inclusion of void porosity induces localized failure with a rapid loss of rigidity which causes an almost vertical descent of the load–displacement curve.

This localization effect can be seen in Figures 8 and 9 where the distributions of thickness and radial strains and of the void porosity along the sheet for different punch travels (every 0·1 in) are plotted. It is worth noting that numerical results for the strain distributions for $f_0 = 0{\cdot}01$ and $k = 0{\cdot}0$ (Figure 8(a)) coincide with those for $f_0 = 0{\cdot}0$ and $k = 0{\cdot}0$ and agree with those reported in Reference 19. Also note that for this case the porosity does not grow over a value of 0·06 and very high values of the thickness strain are obtained ($\simeq 100$ per cent for a

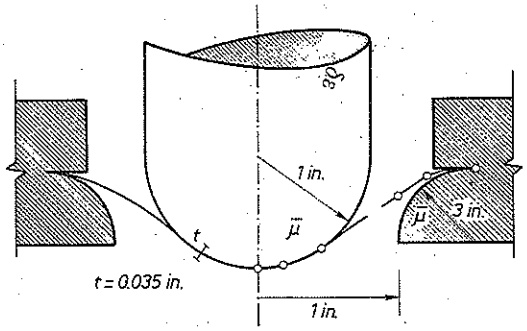

Figure 6. Hemispherical punch stretching. Geometry of punch and blank

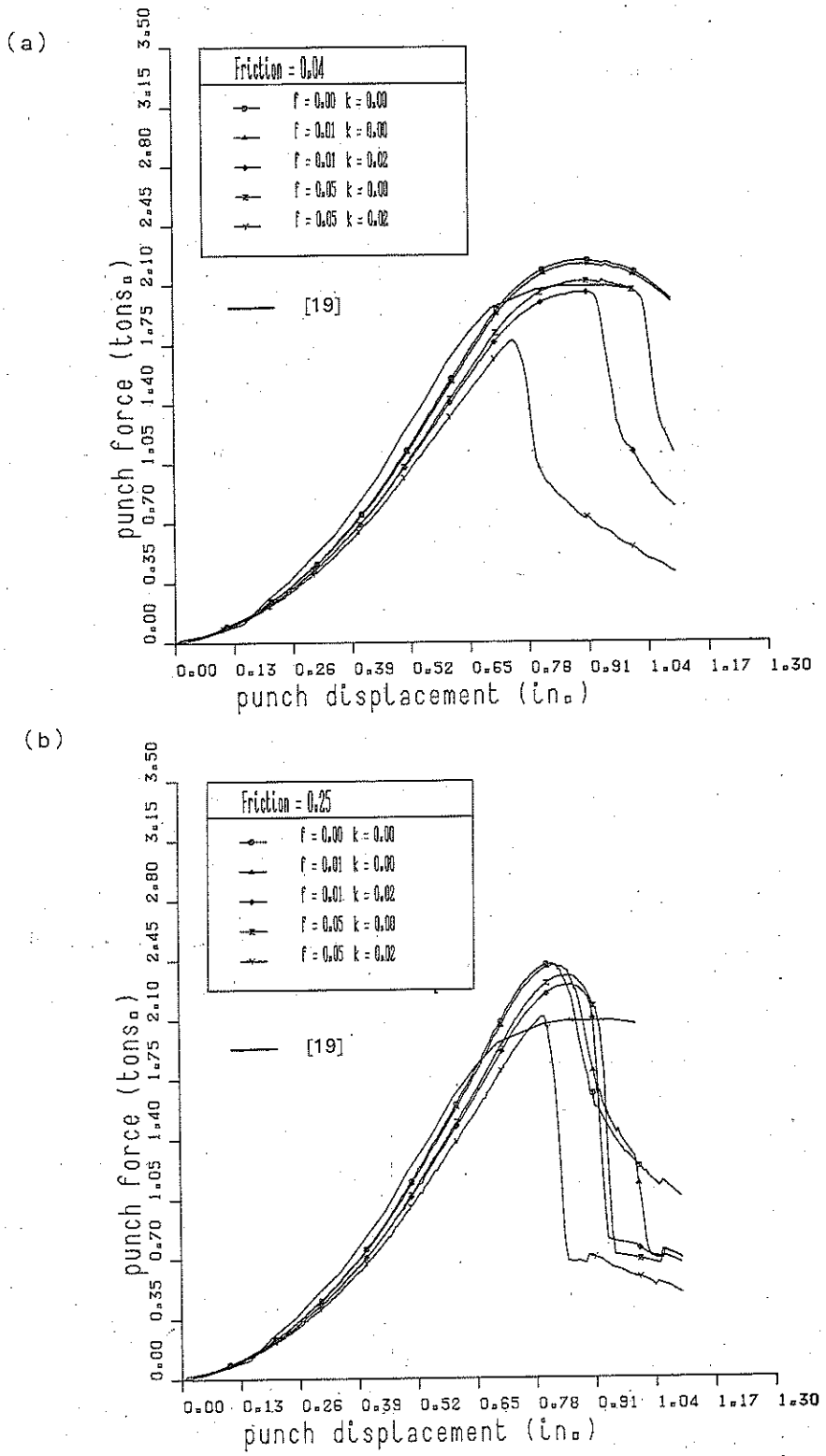

Figure 7. Punch load–travel curves for various friction coefficients, void volume fractions and stress-controlled nucleation parameter (a) $\bar{\mu} = 0{\cdot}04$, (b) $\bar{\mu} = 0{\cdot}25$

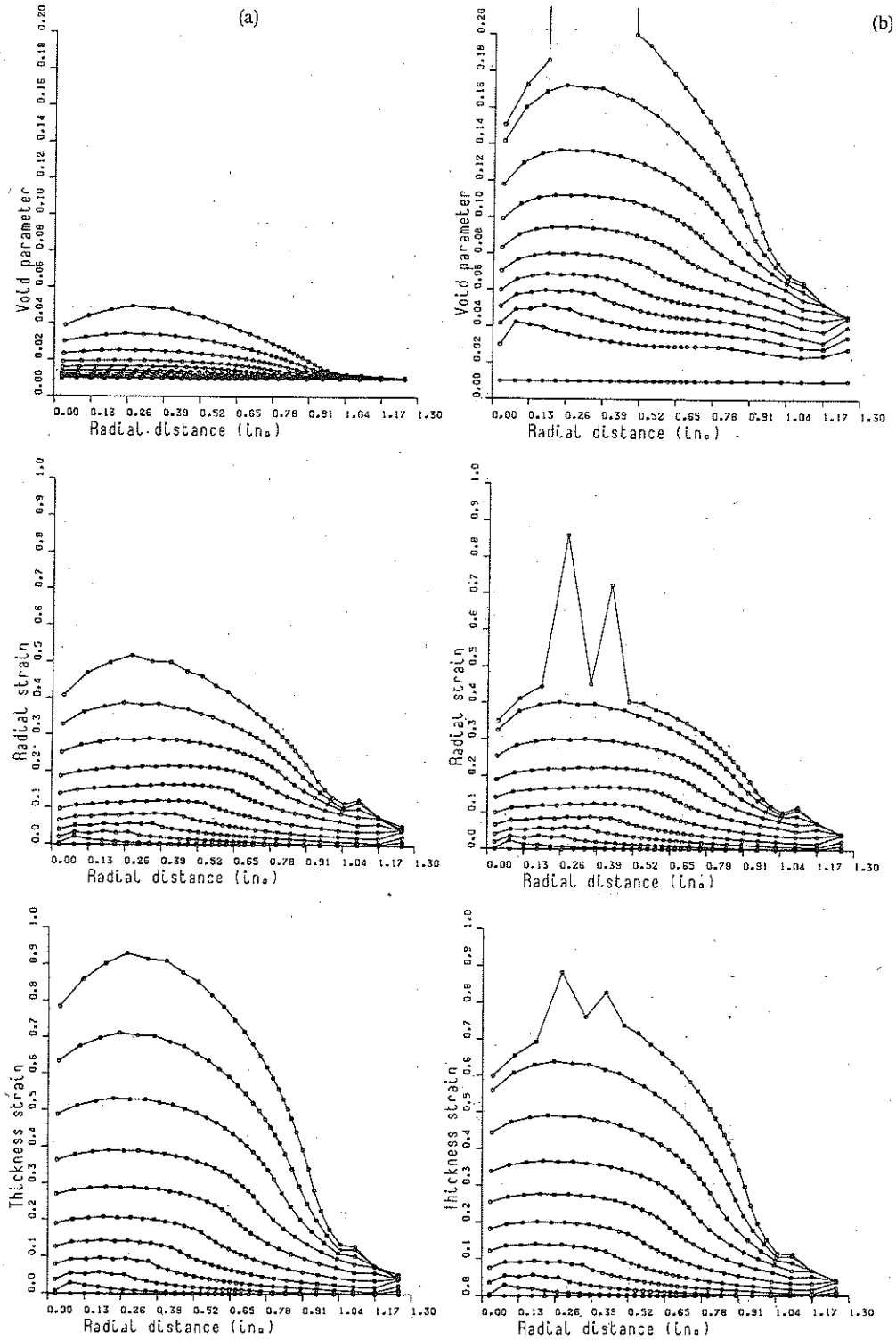

Figure 8. Porosity and strain distributions for $\bar{\mu} = 0{\cdot}04$ and $f = 0{\cdot}01$. All curves plotted for punch travel increments $= 0{\cdot}1$ in: (a) $k = 0{\cdot}0$; (b) $k = 0{\cdot}02$

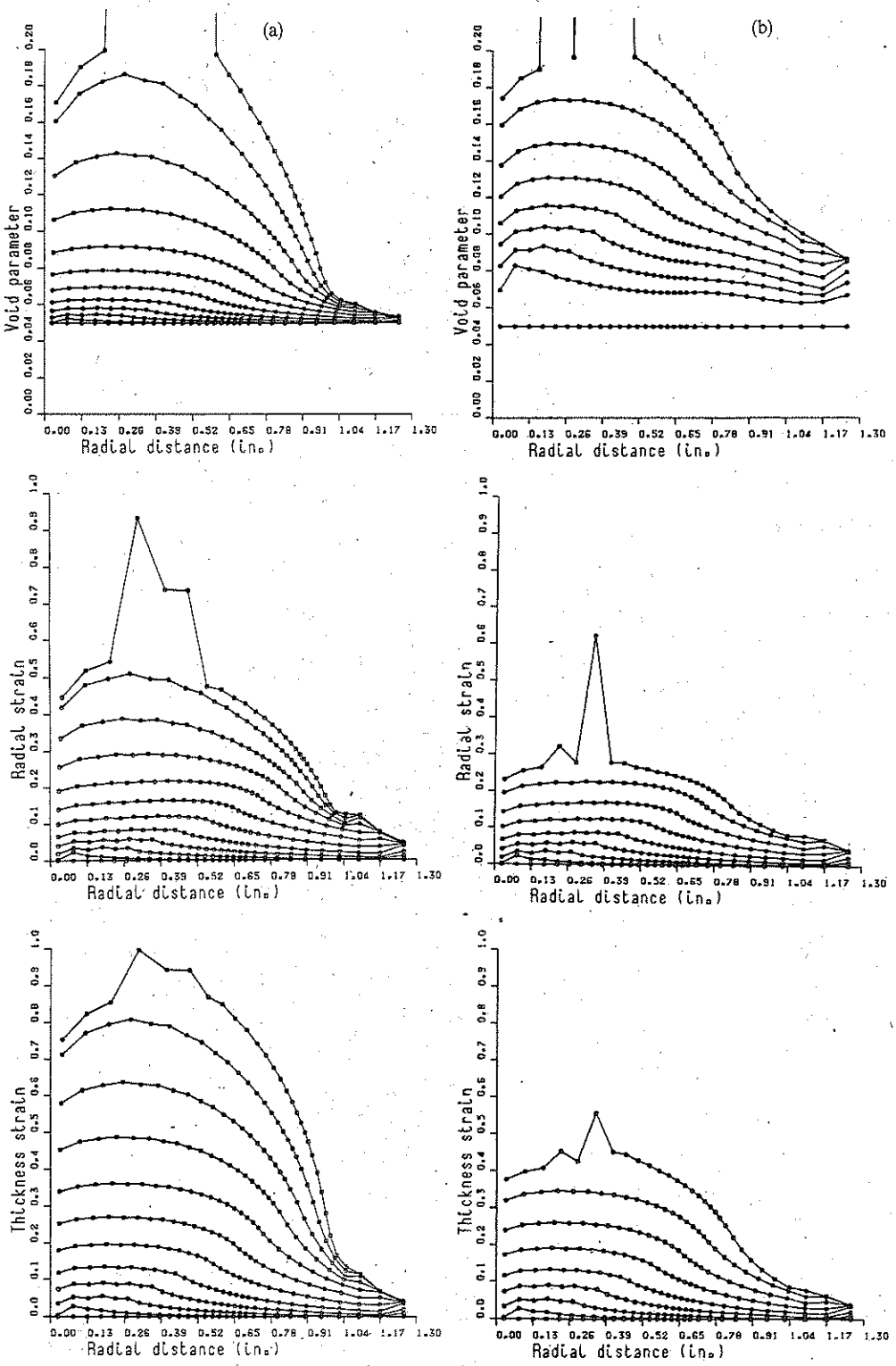

Figure 9. Porosity and strain distributions for $\bar{\mu} = 0{\cdot}04$ and $f = 0{\cdot}05$. All curves plotted for punch travel increments = 0·1 in: (a) $k = 0{\cdot}0$; (b) $k = 0{\cdot}02$

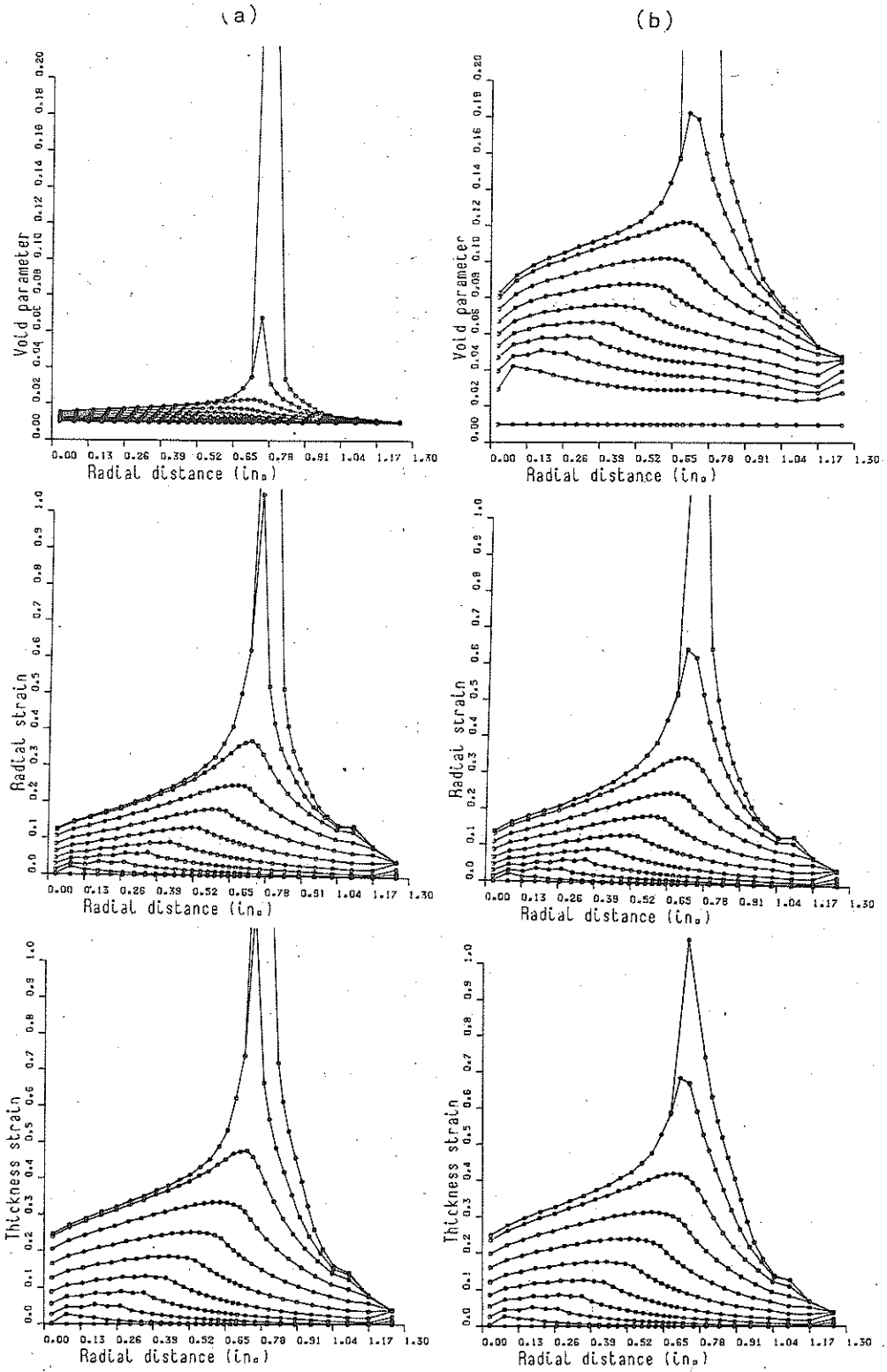

Figure 10. Porosity and strain distributions for $\bar{\mu} = 0{\cdot}25$ and $f = 0{\cdot}01$. All curves plotted for punch travel increments = 0·1 in: (a) $k = 0{\cdot}0$; (b) $k = 0{\cdot}02$

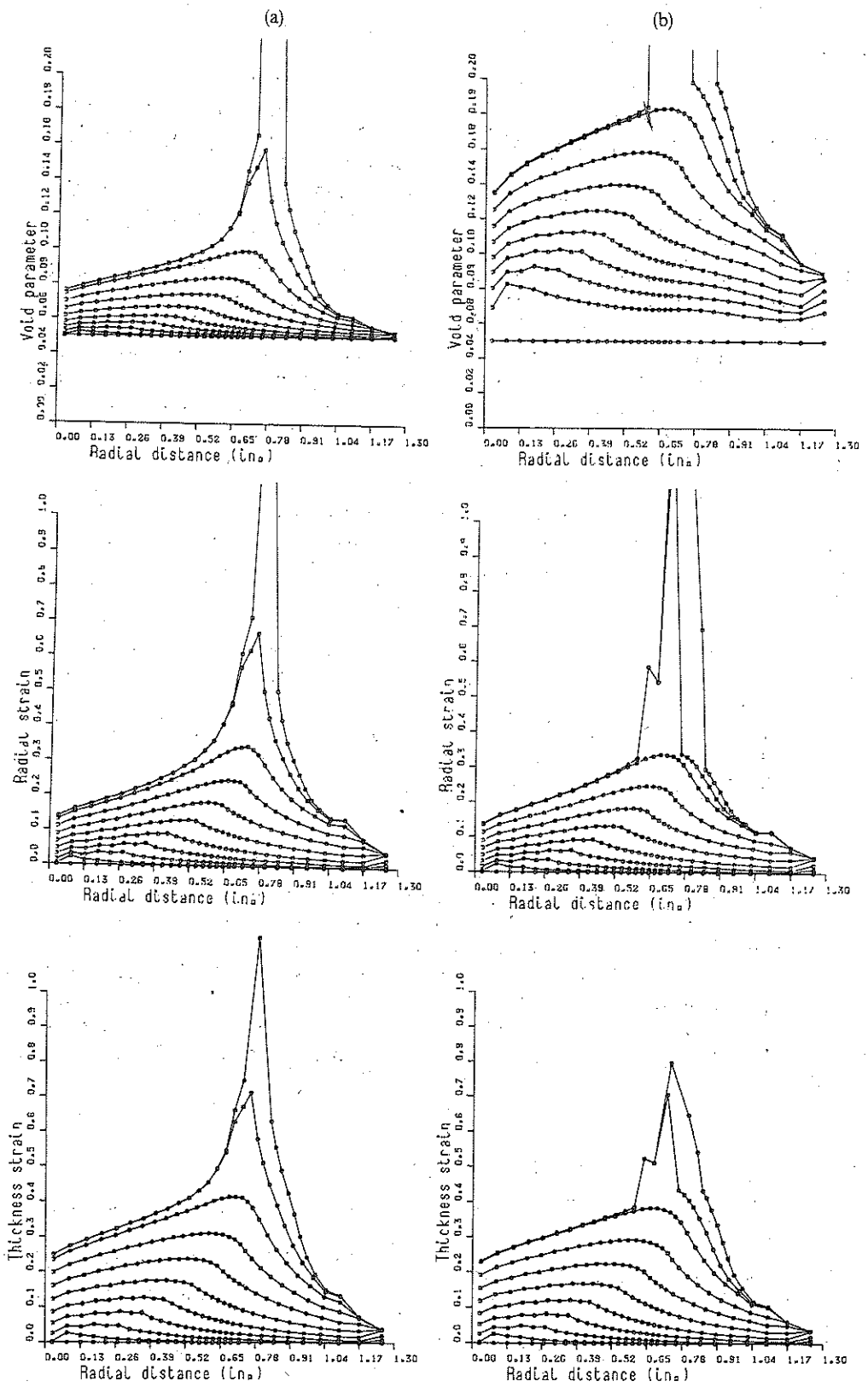

Figure 11. Porosity and strain distributions for $\bar{\mu} = 0{\cdot}25$ and $f = 0{\cdot}05$. All curves plotted for punch travel increments = 0·1 in: (a) $k = 0{\cdot}0$; (b) $k = 0{\cdot}02$

punch travel of 1·0 in). Results are quite different for $f_o = 0{\cdot}01$ and $k = 0{\cdot}02$ (Figure 8(b)). The effect of the nucleation parameter is to increase the growth of porosity which causes strain localization for a punch travel between 0·90 and 1·0 in and a value of the thickness strain of 60 per cent. Figure 8(b) shows clearly the localized failure zone, which corresponds roughly to that of maximum strain. Also note that localization starts for values of $f \simeq 0{\cdot}17$, which agrees well with experimental evidence.[15] This effect is again reproduced for values of the initial porosity of 0·05. Thus, for $f_o = 0{\cdot}05$ and $k = 0{\cdot}0$ (Figure 9(a)) we see that the increase of porosity causes a considerable reduction in the thickness strain, i.e. for a punch travel of 1·0 in. the maximum thickness strain reaches 80 per cent, whereas it reached almost 100 per cent for the case $f_o = 0{\cdot}01$, $k = 0{\cdot}0$ (see Figure 8(a)). On the other hand, the radial strain is almost the same in those two cases. Figure 9(a) shows that strain localization occurs abruptly for a punch travel just greater than 1·0 in.. Note that the maximum porosity at that stage has almost reached the critical value of 20 per cent, which activates the onset of void coalescence. Finally, numerical results obtained for the high values of $f_o = 0{\cdot}05$ and $k = 0{\cdot}02$ (Figure 9(b)) clearly show the rapid increase in porosity to its critical value. This causes early strain localization for a punch travel of $\simeq 0{\cdot}8$ in. and a reduction of the maximum thickness strain of $\simeq 40$ per cent.

The second example corresponds to the same problem with a friction coefficient of 0·25. Numerical results obtained for the punch load–displacement curves for this case (see Figure 7(b)) again show a progressive reduction of the maximum load as the initial porosity and the nucleation parameter increase. However, the differences in the values of the maximum punch load for all cases are not so significant as in the previous example owing to the high strain localization induced by friction which causes in all cases failure at punch travels of $\simeq 0{\cdot}8$ in.. This effect can be seen in Figures 10 and 11. Note that for $f_o = 0{\cdot}1$ and $k = 0{\cdot}0$ (Figure 10(a)) strain and porosity growth localize at a zone of $r \simeq 0{\cdot}78$ in. where the maximum thickness strain is reached for a punch travel $\simeq 0{\cdot}80$ in.. Thus, localization is clearly detected by the rapid growth of porosity in a narrow band, as shown in Figure 10(a). This effect is reproduced in the same form for higher values of the initial porosity and the nucleation parameter, as can be seen in Figure 11(a) and 11(b).

CONCLUSIONS

The equations which describe plastic and viscoplastic flow of metals including the effects of nucleation, growth and coalescence of voids, are analogous to those of classical non-linear elasticity. This allows standard finite element formulations developed for elastic shell problems to be used for the analysis of complex sheet metal forming processes including the effects of voids.

The examples analysed show that by adjusting parameters such as the value and distribution of the initial void volume fraction and of the fraction of particles converted to voids per unit increase of stress, the model should be able to predict development of voids and localized material failure.

REFERENCES

1. O. C. Zienkiewicz and P. N. Godbole, 'Flow of plastic and viscoplastic solids with special reference to extrusion and forming processes', *Int. j. numer. methods eng.*, **8**, 3–16 (1979).
2. G. C. Cornfield and R. H. Johnson, 'Theoretical predictions of plastic flow in hot rolling including the effect of various temperature distributions', *J. Iron Steel Inst.*, **211**, 567–573 (1973).
3. O. C. Zienkiewicz, P. C. Jain and E. Oñate, 'Flow of solids during forming and extrusion. Some aspects of numerical solutions', *Int. J. Solids Struct.*, **14**, 15–38 (1978).
4. O. C. Zienkiewicz, E. Oñate and J. C. Heinrich, 'A general formulation for coupled thermal flow of metals using finite elements', *Int. j. numer. methods eng.*, **17**, 1497–1514 (1981).
5. E. Oñate and O. C. Zienkiewicz, 'A viscous shell formulation for the analysis of thin sheet metal forming', *Int. J. Mech. Sci.*, **25**, 305–335 (1983).

6. E. Oñate and R. Perez Lama, 'Possibilities of the finite element viscous shell approach for analysis of sheet metal forming problems', in *Simulation of Metal Forming Problems by the Finite Element Method* in SIMOP-I held in Stuttgart in 1985, Springer-Verlag, Berlin, 1986.
7. J. F. T. Pittman, O. C. Zienkiewicz, R. D. Wood and J. M. Alexander (eds.), *Numerical Analysis of Forming Processes*, Wiley, New York, 1984.
8. A. L. Gurson, 'Continuum theory of ductile rupture by void nucleation and growth. I. Yield criteria and flow rules for porous ductile media', *J. Eng. Mater. Tech.*, **99**, 2–15 (1977).
9. A. Neddleman and J. R. Rice, 'Limits to ductility set by plastic flow localization', in D. P. Koistinen *et al.*, (eds.), *Mechanics of Sheet Metal Forming*, 1978, pp. 237–266.
10. V. Tvergaard, 'On localization in ductile materials containing spherical voids', *Int. J. Fracture*, **18**, 237–252 (1982).
11. M. Kleiber, 'Numerical study on necking type bifurcations in void containing elastic plastic material', *Int. J. Solid Struct.*, **20**, 191–210 (1984).
12. V. Tvergaard and A. Needleman, 'Analysis of the cup cone fracture in a round tensile bar', *Acta Metall.*, **32**, 157–169 (1984).
13. M. Kleiber, 'On plastic localization and failure in plane strain and round void containing tensile bars', *Int. J. Plasticity* **2**, 205–221 (1986).
14. M. Kleiber, 'Formulations and computational strategies for novel problems of plasticity and creep', *Nucl. Eng. Des.*, **79**, 321–341 (1984).
15. P. S. Theocaris, 'Yield criteria based on void coalescence mechanisms', *Int. J. Solids Struct.*, **22**, 445–466 (1986).
16. C. C. Chu, 'An analysis of localized necking in punch stretching', *Int. J. Solid Struct.*, **16**, 913–931 (1980).
17. O. C. Zienkiewicz, J. Bauer, K. Morgan and E. Oñate, 'A simple and efficient shell element for axisymmetric shells', *Int. j. numer. methods eng.*, **11**, 1545–1559 (1977).
18. J. M. V. Baynham and O. C. Zienkiewicz, 'Developments in the finite element analysis of thin sheet drawing and direct redrawing processes using the rigid plastic approach', in J. F. T. Pittman *et al.* (eds.), *Proceedings of International Conference on Numerical Methods in Industrial Forming Processes*, Pineridge Press, Swansea, 1982.
19. D. M. Woo, 'The stretch forming test', *Engineer*, **220**, 876–889 (1965).